ACS Catalysis

Research Article

pubs.acs.org/acscatalysis

Advantages of $MgAlO_x$ over γ-Al_2O_3 as a Support Material for Potassium-Based High-Temperature Lean NO_x Traps

Jinyong Luo,[†] Feng Gao, Ayman M. Karim,[‡] Pinghong Xu, Nigel D. Browning, and Charles H. F. Peden*

Institute for Integrated Catalysis, Pacific Northwest National Laboratory, Richland, Washington 99354, United States

ABSTRACT: $MgAlO_x$ mixed oxides were employed as supports for potassium-based lean NO_x traps (LNTs) targeted for high-temperature applications. Effects of support compositions, K/Pt loadings, thermal aging, and catalyst regeneration on NO_x storage capacity were systematically investigated. The catalysts were characterized by XRD, NO_x-TPD, TEM, STEM-HAADF, and in situ XAFS. The results indicate that $MgAlO_x$ mixed oxides have significant advantages over conventional γ-Al_2O_3 supports for LNT catalysts, in terms of high-temperature NO_x trapping capacity and thermal stability. First, as a basic support, $MgAlO_x$ stabilizes stored nitrates (in the form of KNO_3) to much higher temperatures in comparison to mildly acidic γ-Al_2O_3. Second, $MgAlO_x$ minimizes Pt sintering during thermal aging, which is not possible for γ-Al_2O_3 supports. Notably, combined XRD, in situ XAFS, and STEM-HAADF results indicate that Pt species in the thermally aged Pt/$MgAlO_x$ samples are finely dispersed in the oxide matrix as isolated atoms. This strong metal−support interaction stabilizes Pt and minimizes the extent of sintering. However, such strong interactions result in Pt oxidation via coordination with the support so that NO oxidation activity can be adversely affected after aging, which in turn decreases NO_x trapping ability for these catalysts. Interestingly, a high-temperature reduction treatment regenerates essentially full NO_x trapping performance. In fact, regenerated Pt/K/$MgAlO_x$ catalyst exhibits much better NO_x trapping performance than fresh Pt/K/Al_2O_3 LNTs over the entire temperature range investigated here. In addition to thermal aging, Pt/K loading effects were systemically studied over the fresh samples. The results indicate that NO_x trapping is kinetically limited at low temperatures, while it is thermodynamically limited at high temperatures. A simple conceptual model was developed to explain the Pt and K loading effects on NO_x storage. An optimized K loading, which allows balancing between the stability of nitrates and exposed Pt surface, gives the best NO_x trapping capability.

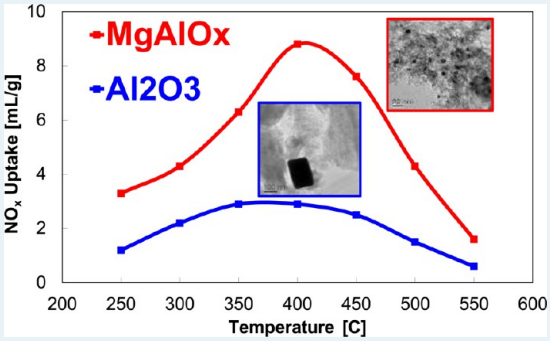

KEYWORDS: *potassium, $MgAl_2O_4$, lean NO_x trap, Pt sintering, thermal aging*

1. INTRODUCTION

Lean NO_x trap (LNT) catalysts are highly efficient for the reduction of NO_x from lean-burn engine exhaust, and this technology was commercialized in 2007 on Cummins diesel engine aftertreatment systems. Typical LNTs consist of three components: a noble-metal catalyst element (typically Pt) for NO oxidation and nitrate reduction, a basic oxide (e.g., BaO) for NO_x storage as nitrates/nitrites, and a high-surface-area support material, such as γ-Al_2O_3.[1] In commercial catalysts, other components such as Pd, Rh, and CeO_2 (or $Ce_xZr_{1-x}O_2$) may also be formulated to further improve performance and durability.[2] Conventional Pt/BaO/Al_2O_3-based LNTs work especially efficiently in the temperature range from 250 to 400 °C. However, their application at higher temperatures such as between 400 and 500 °C encountered, for example, in gasoline direct injection (GDI) engine exhaust, is limited by the thermal stability of stored nitrates.[3,4] Therefore, there is a significant interest in developing LNTs for high-temperature NO_x trapping.

In order to improve the high-temperature performance of LNTs, compositional modifications can be made to the main storage components and/or the support materials. For storage components, the thermal stability of related nitrates plays a crucial role. A number of studies have demonstrated that potassium-based LNTs store much more NO_x than conventional Ba-based LNTs at temperatures of 400 °C and above, due mainly to the enhanced thermal stability of K-nitrates. This enhancement is attributed to the stronger basicity of K in comparison to Ba.[5] In this sense, potassium is a better choice for high-temperature LNTs, although further improvement to address potential issues such as volatility/leaching of K species at high temperatures is certainly needed.[6]

The support materials can also be tailored, since they can affect the stability of the stored nitrates. In addition to the most commonly used γ-Al_2O_3, other materials, such as La_2O_3, CeO_2, CeO_2/Al_2O_3, TiO_2-ZrO_2, Al_2O_3-ZrO_2-TiO_2, K-titanates ($K_2Ti_2O_5$, $K_2Ti_8O_x$), and $MgAl_2O_4$, have been employed as supports.[7−11] Specifically, in order to guarantee an improved performance at high temperatures, the support materials should display at least two important characteristics. First, the support

Received: March 13, 2015
Revised: June 1, 2015
Published: July 2, 2015

DOI: 10.1021/acscatal.5b00542
ACS Catal. 2015, 5, 4680−4689

materials should stabilize the trapped nitrates. Results from the recent literature indicate that, with the more basic $MgAl_2O_4$ spinel as a support instead of (mildly acidic) γ-Al_2O_3, the high-temperature performance of both Ba- and K-based LNTs can be enhanced.[11,12] Second, the support materials should be able to improve the thermal aging resistance of the catalysts. Practically this is very important, since LNTs are susceptible to sulfur poisoning in operations and, therefore, must undergo periodic high-temperature desulfation/regeneration. Preliminary results indicate that desulfation temperatures as high as 800 °C may be required for K-based LNTs.[4] At such high temperatures, the Pt LNT component may experience irreversible sintering. In this regard, finding support materials that are capable of preventing Pt from sintering is especially important for practical applications.

According to the recent literature, several support materials, including $CaTiO_3$, CeO_2 ,and MgO, show considerable potential for Pt stabilization due to strong Pt−support interactions.[13−15] For example, in the so-called intelligent $CaTi_{0.95}Pt_{0.05}O_3$ catalyst, it has been reported that Pt forms a solid solution with the support and can diffuse in and out of the perovskite structure depending on changes in the gaseous environment.[13] For CeO_2 and MgO, thanks to the formation of Pt−O−Ce or Pt−O−Mg linkages as confirmed by EXAFS studies,[14,15] the support can serve as especially strong anchoring sites for Pt atoms, which prevents Pt from sintering. Among these supports, MgO appears to be a good candidate for high-temperature LNTs, considering that its basicity will also help stabilize the stored nitrates. However,the low specific surface area of pure MgO, especially after high-temperature treatments, limits its application. Doping MgO with Al_2O_3 can resolve this issue, as the formed $MgAlO_x$ mixed oxides have higher surface area, good basicity, and excellent thermal stability. In fact, these latter materials have already been incorporated into commercial Ba-based LNT formulations.[2] Very recently, it has been found that high-surface-area $MgAl_2O_4$ is capable of stabilizing platinum nanoparticles on the relatively abundant {111} facets, where Pt nanoparticles <2 nm even survive especially harsh aging conditions, such as 800 °C in air for 1 week.[16] Therefore, $MgAlO_x$ mixed oxides are chosen here as supports for K-based high-temperature LNTs. Although use of $MgAl_2O_4$ spinel as a support for LNTs has already been reported,[11,12] little is known about their thermal stability, such as Pt dispersion and sintering behaviors in response to aging. In this study we show that these mixed oxides have much improved capability for Pt stabilization under thermal aging conditions, in comparison to conventional γ-Al_2O_3 supports, thereby making them promising supports for commercial high-temperature LNTs.

2. EXPERIMENTAL SECTION

2.1. Catalyst Preparation. $MgAlO_x$ mixed oxides were prepared by calcination of commercial hydrotalcite precursors, (Sasol) Pural MG30 (Mg/Al = 0.6), MG50 (Mg/Al = 1.4), and MG70 (Mg/Al = 3.0), at 600 °C for 4 h in air (BET surface areas are 250, 200, and 180 $m^2\ g^{-1}$, respectively, for the calcined materials). Pt (1 wt %) was loaded by incipient wetness impregnation onto these mixed oxides and a γ-Al_2O_3 support (Alfa Aesar, 150 $m^2\ g^{-1}$) with a dilute $Pt(NH_3)_4(NO_3)_2$ (Alfa Aesar) solution at room temperature. After drying and calcination at 500 °C for 4 h in air, these materials were subsequently impregnated with K_2CO_3 (Alfa Aesar) solutions to give varying K loadings. Fresh catalysts were obtained via drying at ambient temperature and calcination at 600 °C for 4 h. In order to investigate thermal aging effects, the catalysts were treated at 800 °C for 4 h in air. After thermal aging, some catalysts were reduced again in 4% H_2/He (the feed also contained 5% CO_2 and 5% H_2O) at 800 °C for 1 h. The catalysts are denoted as xK/yPt/support, where x and y are the weight percentages of supported K and Pt, respectively.

2.2. LNT Performance. NO_x storage capacity measurements have been described in detail elsewhere.[17] Briefly, a 120 mg sample was loaded in a quartz tube microreactor (o.d. 1/2 in.) and tested from 550 to 250 °C at 50 °C intervals. For each test, the catalyst was conditioned by 20 lean/rich (L/R) cycles (L/R = 50/10 s; lean gas 150 ppm of NO, 5% O_2, 5% CO_2, 5% H_2O, balanced by He; rich gas 4% H_2, 5% CO_2, 5% H_2O balanced by He) to ensure that a steady cycle to cycle performance was achieved. Thereafter, continuous lean gas was introduced and outlet NO_x concentrations were monitored by a chemiluminescence NO_x analyzer (Thermo Electron, 42C) until output levels reach 60 ppm (i.e., 40% of the input NO_x concentrations), and the NO_x trapping capacity was measured by the amount of NO_x stored during this period. The total gas flow rate was 400 mL/min, corresponding to a weight hourly space velocity of 200000 mL $g^{-1}\ h^{-1}$.

2.3. Catalyst Characterization. Catalyst characterization, including temperature-programmed desorption of NO_x (NO_x-TPD), reactivity for NO oxidation, powder X-ray diffraction (XRD), and transmission electron microscopy (TEM), is described in detail elsewhere.[17] Briefly, NO_x-TPD was performed by saturating 50 mg of powder samples with 0.5% NO_2/He at room temperature for 1 h, purging with He (200 mL/min) for 2 h, and finally ramping the temperature to 800 °C at a linear rate of 5 °C/min. NO and NO_2 desorption was monitored using the same NO_x analyzer mentioned above. Steady-state NO oxidation was measured by flowing 150 ppm of NO, 5% O_2, 5% CO_2, 5% H_2O, balanced He through the powder samples at a weight hourly space velocity of 800000 mL $g^{-1}\ h^{-1}$. The sample was heated stepwise from 250 to 550 °C at increments of 50 °C.

XRD was performed on a PANalytical X'Pert system operating at 40 kV, 50 mA, using Cu Kα radiation (λ = 0.154 nm). The data were recorded from 10 to 70° (2θ) with a step size of 0.04°. TEM was carried out on a JEOL JEM 2010 instrument operating at 200 kV. Samples were prepared by depositing the powdered samples suspended in ethanol (ultrasonic treatment) on a carbon-coated copper grid. Scanning-TEM high angle annular dark field (STEM-HAADF) samples were prepared by dipping a 200 mesh lacey-carbon Cu grid (Ted-Pella) into the initially prepared catalyst powder. Samples were imaged with an aberration-corrected FEI Titan 80/300S instrument operating at 300 keV. The convergence semiangle was 17.8 mrad with an HAADF collection inner angle of ∼75 mrad.

The catalysts were also characterized by in situ Pt L_3-edge X-ray absorption spectroscopy (XAS) using an in-house-built cell with 4 mm i.d. glassy-carbon tubing.[18] The XAS measurements were performed at beamline X-18A at the National Synchrotron Light Source (NSLS) operated by the Synchrotron Catalysis Consortium (SCC) at Brookhaven National Laboratory. The catalyst was reduced in 100% H_2 flow (50 SCCM) at 450 °C with a ramping rate of 10 °C/min for 2 h and then cooled to room temperature. The extended X-ray absorption fine structure (EXAFS) spectra were collected at room temperature under 100% H_2 flow. XANES and EXAFS data processing and analysis were performed using Athena and

DOI: 10.1021/acscatal.5b00542
ACS Catal. 2015, 5, 4680−4689

Artemis programs of the IFEFFIT data analysis package.[19,20] For each catalyst and set of conditions, three scans were collected and merged after alignment using a Pt-foil spectrum collected simultaneously for each scan. $\chi(k)$ (where k is the photoelectron wavenumber) was obtained by subtracting smooth atomic background from the normalized absorption coefficient using the AUTOBK code. The theoretical EXAFS signal was constructed using the FEFF6 code[21] and fitted to the data in r space using the Artemis program of the IFEFFIT package. For Pt, we used an fcc crystal structure with a lattice constant of 3.92 Å. The Pt−K scattering path was calculated from an $Na_2Pt(OH)_6$ structure where the Na atoms were replaced with K. This choice of Pt and K containing structure was made in order to generate a Pt−K bond distance of 3.36 Å that matches the distance expected for Pt−K reported for $PtK_6O_4(OH)_2$ and PtK_6[22] (bond distances were obtained through private communication with Prof. Manos Mavrikakis). The Pt−Mg/Al and Pt−O scattering paths were calculated from an $MgAl_2O_4$ structure by replacing one Mg atom with Pt. The theoretical EXAFS signals were fitted to the data in r space using the Artemis program of the IFEFFIT package. The spectra were fitted by varying the coordination number of the single scattering Pt−Pt, Pt−O, Pt−K, and Pt−Mg paths, the bond length disorder (Debye−Waller factor), and the effective scattering lengths for each path and the correction to the threshold energy, ΔE_0. S_0^2 (the passive electron reduction factor) was obtained by first analyzing the spectrum for a Pt foil, and the best fit value (0.85) was fixed during the fitting. The k range used for Fourier transform of $\chi(k)$ was 3−16 $Å^{-1}$, and the r range for fitting was 1.3−3.2 Å.

3. RESULTS AND DISCUSSION

3.1. Support Effects. *3.1.1. NO_x Trapping Performance.* NO_x trapping performance as a function of temperature for fresh catalysts with identical Pt (1 wt %) and K (10 wt %) loadings but on different supports is shown in Figure 1. With increasing temperature, a general trend for each catalyst is that NO_x storage capacity first increases, reaches a maximum, and finally decreases at the highest temperatures due to the limited stability of stored NO_x. Clearly evident from Figure 1 is that the $MgAlO_x$-based catalysts show improved high-temperature performance relative to the γ-Al_2O_3-supported catalysts, especially at 500 °C and above. Among the three $MgAlO_x$-based catalysts, the MG30-supported catalyst exhibits the best performance. In the following text, only the MG30 support, among $MgAlO_x$, is studied in detail.

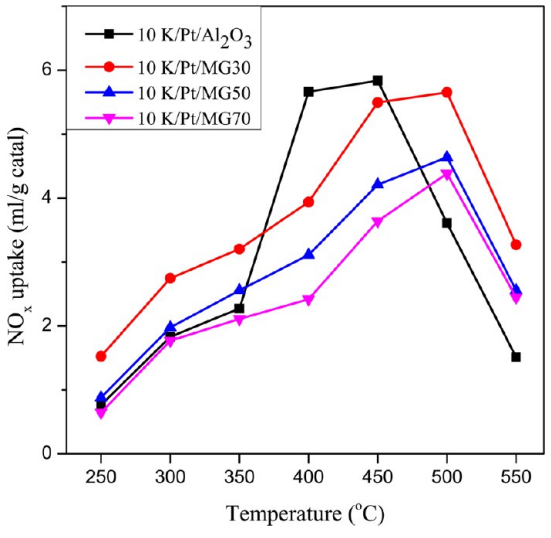

Figure 1. NO_x uptake performance for catalysts prepared on different support materials.

3.1.2. NO_x-TPD. At high temperatures, the stored NO_x, in the form of nitrates,[23] tends to decompose; therefore, the stability of the stored nitrates determines the high-temperature NO_x trapping performance. Clear differences in maximum NO_x storage temperatures shown in Figure 1 suggest that the support materials influence the stability of the nitrates. In order to measure the nitrate stability, NO_x-TPD was performed for the 10K/Pt/Al_2O_3 and 10K/Pt/MG30 samples, and the results are shown in Figure 2 for direct comparison. Three NO_x desorption peaks are detected for each sample.[12,17,24] The low-temperature peaks (<200 °C, NO_2 only) are assigned to the desorption of weakly adsorbed NO_x, while the intermediate temperature peaks (centered at ∼468 °C for MG30 and ∼415 °C for Al_2O_3, mostly NO_2) are attributed to decomposition of surface nitrates interacting strongly with the support. The high-temperature NO_x peaks (580 °C for MG30 and 520 °C for Al_2O_3, NO only) are due to decomposition of bulklike KNO_3 that interacts less strongly with the support materials. Clearly, the decomposition temperatures of both types of KNO_3 are ∼50−60 °C higher on 10K/Pt/MG30, in comparison with 10K/Pt/Al_2O_3. This is consistent with the performance results illustrated in Figure 1, where the high-temperature trapping window for the MG30-based sample is enhanced by ∼50 °C in comparison with the Al_2O_3-based sample.

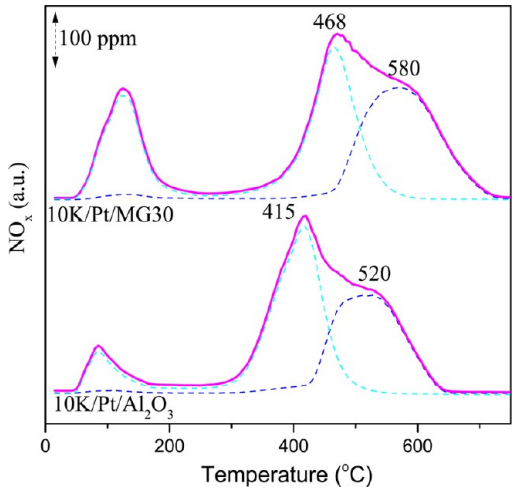

Figure 2. NO_x-TPD profiles for the 10K/Pt/Al_2O_3 and 10K/Pt/MG30 samples (solid line, NO_x; dashed cyan line, NO_2; dashed blue line, NO).

3.1.3. Discussion on Nitrate Stability. Next, the origins for the nitrate stability enhancement on $MgAlO_x$, in comparison with Al_2O_3, are discussed. The bulk K-nitrate decomposition process is described first. According to the literature, the decomposition of nitrates is initiated via dissociation of one of the three equivalent N−O bonds.[23] The weaker the N−O bonds are, the more readily nitrates decompose. The N−O bond strength can be weakened by metal cations via electronic polarization. The extent of polarization is dependent on the charge density (CD) of the metal cation, which is defined as the ratio of effective charge to the volume of a metal cation.[25]

DOI: 10.1021/acscatal.5b00542
ACS Catal. 2015, 5, 4680−4689

Therefore, for bulk nitrates with different metal cations, a higher CD value of the metal cation generally corresponds to a lower decomposition temperature of the nitrates. For example, Al^{3+} has a very high CD value of 4.8×10^{-3} e/nm^3 and, correspondingly, $Al(NO_3)_3$ decomposes at very low temperature (<200 °C) because of strong polarization. In contrast, K^+ has a very low CD value of 7×10^{-5} e/nm^3 and, as a result, the decomposition temperature of bulk KNO_3 is very high (>800 °C). We note that this is higher than that for $Ba(NO_3)_2$ (~700 °C), and this is a key factor in explaining why K has the advantage over Ba as a storage component for high-temperature LNTs.

If the nitrates are present as two-dimensional structures on the support surface, the N−O bonds can also be affected by the exposed cations from the support, such as surface Al^{3+} from Al_2O_3. Previous studies on the $Ba(NO_3)/Al_2O_3$ system indicated that there exist strong interactions or even bonding between nitrates (including both surface and bulklike nitrates) and the support surface cations.[26] Therefore, it can be suggested that direct polarization of the N−O bonds strongly interacting with the support leads to the promoted decomposition of nitrates; in general, this explains why surface nitrates usually decompose at temperatures lower than those for bulklike nitrates. Considering the lower charge density of Mg^{2+} (7.5×10^{-4} e/nm^3) in comparsion to Al^{3+} (4.8×10^{-3} e/nm^3), it is expected that surface nitrates supported on $MgAlO_x$ are more stable than those on Al_2O_3.[25] Indeed, both LNT performance results shown in Figure 1 and NO_x-TPD results shown in Figure 2 are fully consistent with this picture.

3.2. K and Pt Loading Effects. *3.2.1. NO_x Trapping Performance.* Since MG30 performs the best for the high-temperature NO_x trapping among $MgAlO_x$ supports, it was chosen to investigate effects of K and Pt loadings. Figure 3a shows the amounts of NO_x trapped over MG30-based catalysts at various K loadings (Pt loading fixed at 1 wt %). With increasing K loadings from 2 to 15%, the optimum operating window at which a maximum NO_x trapping could be obtained shifts to higher temperatures. Consequently, the high-temperature (i.e., 450 °C and above) NO_x trapping capacity increases. However, further increasing K loading from 15% to 20% leads to a decrease in NO_x trapping over the entire temperature range, although the optimum operating window is not affected much. Therefore, K loading plays a crucial role in high-temperature NO_x trapping, and there exists an optimum K loading where the best performance can be achieved: i.e., 15 wt % here for MG30. In our previous study of Al_2O_3-supported K LNTs, a very similar trend was observed.[17] In that case, a 10 wt % K loading was found to be the optimum.

Figure 3b shows NO_x uptakes over MG30 catalysts at different Pt loadings (K loading fixed at 10%). Below 450 °C, NO_x uptake increases monotonically with Pt loading, while at higher temperatures, NO_x trapping becomes less dependent on Pt loading. Specifically, all samples exhibit essentially the same NO_x uptakes at 550 °C, regardless of the Pt loading. Note that, at this temperature, NO oxidation to NO_2 catalyzed by Pt is determined by thermodynamics rather than availability of Pt sites.

3.2.2. Schematic Model for NO_x Uptake. In order to better explain the Pt and K loading effects on LNT performance, we developed a simple schematic model for NO_x trapping, as shown in Figure 4a. Note that the NO_x trapping process is initiated by NO oxidation on Pt sites and the formed NO_2 is stored as nitrates by interaction with K. The total storage area

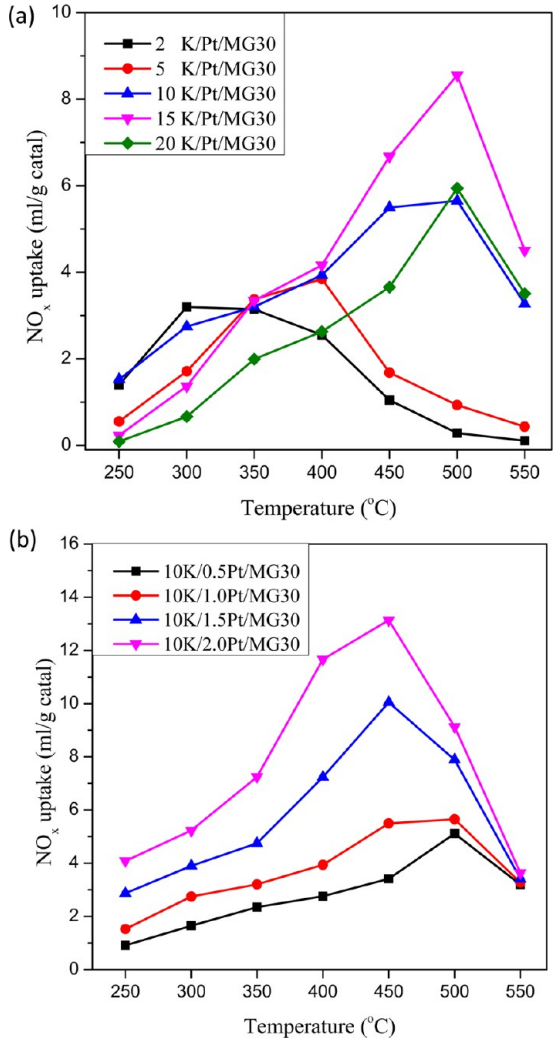

Figure 3. NO_x uptake performance for the MG30-supported catalysts with varying (a) K and (b) Pt loadings.

can be viewed as a combination of multiple storage zones, with each zone being constructed by a Pt particle center surrounded by a K-phase of a finite thickness. The total storage area $\sum_{i=1}^{N_{Pt,K}} S_{i(T)}$ is, therefore, defined by the Pt particle number $N_{(Pt,K)}$ and the individual storage zone $S_{i(T)}$ around each Pt particle. The total NO_x storage capacity (NSC) is determined by the total storage area $\sum_{i=1}^{N_{Pt,K}} S_{i(T)}$ and the average nitrate coverage $\Theta_{(T,K)}$:

$$NSC = \sum_{i=1}^{N_{Pt,K}} S_{i(T)}\Theta_{(T,K)} \quad (1)$$

Next, each parameter is analyzed as a function of Pt/K loadings and temperature. First, the Pt particle number $N_{Pt,K}$ is a function of both Pt and K loadings. For freshly prepared samples with fine Pt dispersions, higher Pt loading corresponds to more exposed Pt particles and higher $N_{Pt,K}$ value. However, excess K can lead to Pt particles being covered or encapsulated, which was confirmed by the low Pt exposure (1%) of the 20K/Pt/Al_2O_3 sample;[17,27] therefore, the Pt particle number $N_{Pt,K}$ will decrease at high K loadings. The storage zone $S_{i(T)}$ around each Pt particle is primarily a function of temperature. This is because higher temperatures promote nitrate diffusion and, thus, storage zone expansion. Such diffusion has been reported

DOI: 10.1021/acscatal.5b00542
ACS Catal. 2015, 5, 4680−4689

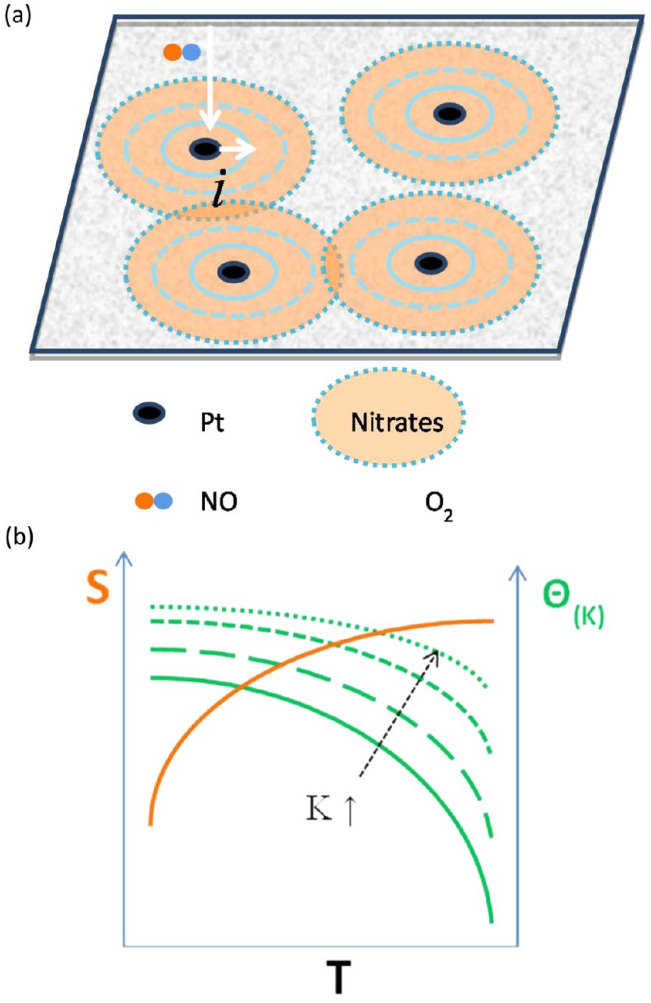

Figure 4. Physical model for NO_x trapping (a) and illustration of the storage area S and nitrate coverage $\Theta_{(K)}$ as a function of temperature and K loadings (b).

in prior literature, especially for storage sites far away from Pt sites (nonproximal sites).[28−30] The effective nitrate coverage $\Theta_{(T,K)}$, which reflects the thermal stability of the stored nitrates and can be considered as a stability term, is a function of temperature and K loading. High temperatures promote nitrate decomposition, thereby decreasing the nitrate coverage, while high K loading enhances the nitrate stability, due to the decreased percentage of surface nitrates which decompose at lower temperatures as discussed above. Note that, during NO_x trapping, a nitrate concentration gradient might be generated around the Pt center: that is, more nitrates form in the proximity of Pt.[31] Therefore, the term $\Theta_{(T,K)}$ here is best viewed as an average coverage.

In the following, the Pt loading effect is first analyzed based on the above model. From eq 1, it is concluded that Pt loading mainly affects the Pt particle number $N_{Pt,K}$. Increasing Pt loading generates more storage zones and, correspondingly, greater total storage area. This is consistent with the enhanced NO_x trapping with increasing Pt loadings at low temperatures, as shown in Figure 3b. However, the dependence of NO_x trapping on Pt loading decreases at higher temperatures and almost disappears at a very high temperature of 550 °C. This phenomenon is explained as follows: at high temperatures, the storage zone $S_{i(T)}$, as illustrated in Figure 4a, is expected to expand due to more facile nitrate diffusion. This leads to overlapping of neighboring storage zones. Therefore, the dependence of the total storage area on Pt loading decreases. It is fully expected that, if the temperature is high enough where nitrate diffusion becomes sufficiently rapid, the whole surface will be utilized for NO_x storage. In this case, the total storage area $\sum_{i=1}^{N_{Pt,K}} S_{i(T)}$ is constant for all samples regardless of the Pt loadings and, according to eq 1, the NSC is only dependent on the NO_x coverage $\Theta_{(T,K)}$, which is a function of K loading. Here, since all the samples have the same K loading, they show exactly the same NO_x trapping capacity at 550 °C.

As to the K loading effect, the primary conclusion to be made from Figure 3a is that the optimum operating temperature shifts to higher temperatures as the K loading increases. First, the existence of the optimum temperature is explained for a fixed K loading: from the discussions above, both the diffusion term $S_{i(T)}$ and the stability term $\Theta_{(T,K)}$ are temperature dependent: with increasing temperature, $S_{i(T)}$ increases while $\Theta_{(T,K)}$ decreases. In Figure 4b, the relationship between these two terms is schematically illustrated as a function of temperature. As expected, the maximum NO_x storage is achieved at a temperature that balances the diffusion rate and thermal stability of the stored nitrates, which is the optimum operating temperature. Second, the impact of K loading on the optimum operating temperature is analyzed. With increased K loading, the thermal stability of the stored nitrates $\Theta_{(T,K)}$ will increase as a result of the decreased interaction with support. As illustrated in Figure 4b, a rebalance of the diffusion and stability terms will push the best operating temperature to higher temperature. Note, however, that as the K loading is increased to a very high level, i.e. from 15 wt % to 20 wt %, the increase in the stability term is very limited and, therefore, the best operating temperature is no longer increased. Instead, the total number of exposed Pt particles, i.e. the $N_{Pt,K}$ term, drops rapidly due to Pt encapsulation by K species. In this case, the availability of Pt limits NO oxidation, leading to the overall decreased performance. Note that such a K loading effect, in terms of nitrate stability and Pt encapsulation, has also been observed for $Pt/K/Al_2O_3$ samples.[17]

3.3. Effects of Thermal Aging and Reductive Regeneration. *3.3.1. NO_x Trapping Performance for Fresh and Aged LNTs.* As mentioned before, the catalyst may experience high-temperature exposure during regenerative desulfation events and, as such, understanding the thermal aging behavior is key to practical application. Figure 5 shows comparative results for NO_x storage as a function of temperature for Al_2O_3- and MG30-based catalysts with the same Pt (1 wt %) and K (10 wt %) loadings, in their fresh (F), aged (A), and aged-reduced (AR) states. Here, aging was conducted at 800 °C for 4 h in air, and subsequent reduction was performed at the same temperature in 4% H_2/He for 1 h. Clearly, thermal aging significantly lowers NO_x storage performance for both catalysts; for example, the amount of NO_x trapped at 500 °C decreases from 5.5 to 1.5 mL/g for the MG30-supported catalyst and from 3.5 to 0.4 mL/g for the Al_2O_3-based catalyst. Still, the MG30-based sample shows better performance than the Al_2O_3-supported catalyst after aging. As noted above, the NO_x storage performance for the aged-reduced samples is also included in Figure 5 but will be addressed in more detail in section 3.3.3 below.

3.3.2. Phase Changes during Aging. To elucidate phase changes during aging, the Al_2O_3- and MG30-supported catalysts (1 wt % Pt and 10 wt % K loading) were analyzed

DOI: 10.1021/acscatal.5b00542
ACS Catal. 2015, 5, 4680−4689

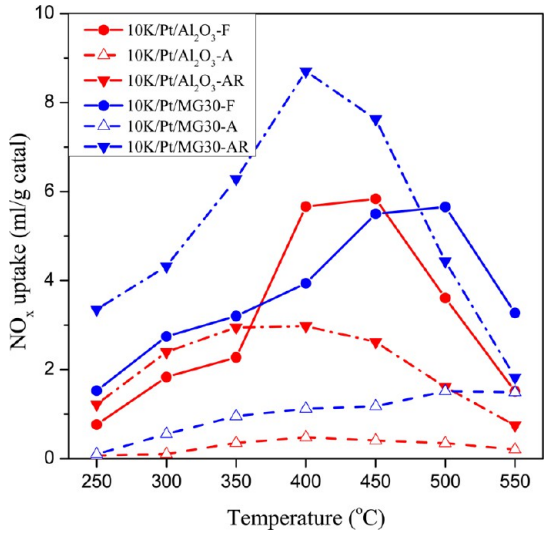

Figure 5. NO_x uptake performance for the fresh (F), aged (A), and aged/reduced (AR) Al_2O_3- and MG30-supported catalysts.

by XRD before and after aging, and the diffraction patterns are shown in Figure 6. The data for the MG30 (Mg/Al = 0.6)

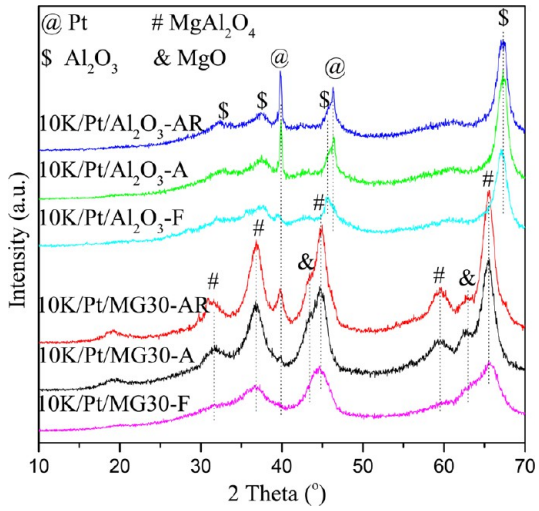

Figure 6. XRD patterns from the fresh (F), aged (A), and aged/reduced (AR) Al_2O_3- and MG30-supported catalysts.

sample are mainly composed of features from $MgAl_2O_4$ spinel, with a small amount of pure MgO phase. The Al_2O_3-based sample exhibits peaks primarily due to γ-Al_2O_3. No K-containing phase can be detected for any of these catalysts, suggesting that potassium species are finely spread on the surfaces of the supports. After aging, all of the diffraction peaks from the supports become sharper, indicating crystallization and particle growth of these phases. However, there exists a striking difference for the Pt phase between the Al_2O_3- and MG30-supported samples after aging. For the Al_2O_3-based sample, sharp and intense Pt diffraction peaks appear after aging, demonstrating Pt sintering. This has been identified as the major degradation mode for this catalyst.[17] Surprisingly, no Pt-metal-related peaks are observed after aging for the MG30-based sample, suggesting that Pt remains highly dispersed. Considering the poor NO_x storage performance of the aged MG30-based sample, it appears that a deactivation mechanism different from Pt sintering, perhaps Pt oxidation, occurs for this catalyst. The colors of the aged samples provide more evidence on differences in deactivation; notably, the aged Al_2O_3-based sample shows a gray color consistent with the presence of metallic Pt particles, while the aged MG30-based sample is white, suggesting an absence of a metallic Pt phase.

In order to further understand the chemical nature of Pt in the aged Al_2O_3- and MG30-supported samples, NO oxidation to NO_2, a reaction very sensitive to the oxidation states of Pt,[32] was carried out over the aged catalysts, and the results are shown in Figure 7. The aged Al_2O_3-based sample shows poor

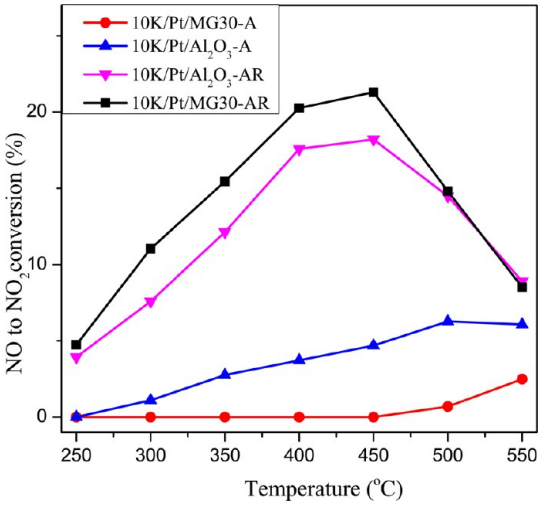

Figure 7. Conversions of NO oxidation to NO_2 over the aged (A) and aged/reduced (AR) Al_2O_3- and MG30-supported catalysts.

NO oxidation activities consistent with Pt sintering. Interestingly, the aged MG30-based sample is completely inactive for NO oxidation even up to 450 °C. On the basis of previous findings that highly dispersed metallic Pt is very active in catalyzing NO oxidation,[33] the XRD and NO oxidation results suggest that Pt is maintained in nonmetallic states in the aged MG30-based sample, which causes catalyst deactivation. In general, NO_x trapping at high temperatures is not determined by NO oxidation, since this step is facile kinetically, but instead by the stability of nitrates as discussed above. However, if NO oxidation is severely inhibited due to a Pt phase change, for example in the case of the aged MG30-based sample, it could become the rate-limiting step for NO_x trapping. Pt phase changes will be further evidenced by the characterization results presented below.

3.3.3. Catalyst Regeneration. Since Pt oxidation is expected to be the major cause of deactivation for aged MG30-based sample, a reduction treatment was performed to regenerate the aged catalyst by exposing the catalyst to a rich-phase gas (4% H_2/He, 5% CO_2, and 5% H_2O) at 800 °C for 1 h. The aged Al_2O_3-based catalyst was treated in the same way for direct comparison. The NO_x trapping performances for the regenerated samples are shown in Figure 5. For both catalysts, the reduction treatment increases the NO_x trapping capacity in comparison to their aged counterparts. For example, the amount of NO_x trapped at 500 °C increases from around 0.4 to 1.5 mL/g for the Al_2O_3-based sample and from around 1.5 to 4.4 mL/g for the MG30-based catalyst, an almost 3-fold improvement in this case. In comparison with the fresh catalysts, the aged-reduced MG30-supported catalyst recovers

DOI: 10.1021/acscatal.5b00542
ACS Catal. 2015, 5, 4680−4689

~80% of the NO_x trapping capacity at 500 °C, while the aged-reduced Al_2O_3-based sample only recovers ~40%. Overall, after a high-temperature reduction treatment, the MG30-based sample shows great advantages over the Al_2O_3-supported catalyst, as it also shows much better performance over the entire temperature range studied here.

The XRD patterns for the aged-reduced catalysts are also shown in Figure 6. No significant differences were found for the aged Al_2O_3-based samples before and after reduction. For the MG30-supported catalysts, broad and weak metallic Pt diffraction peaks appear after reduction. From the width of the Pt diffraction peak at 39.7°, the average Pt particle size is estimated to be ~7.3 nm using the Scherrer equation. To further elucidate the nature of Pt species, TEM was performed on the aged and aged-reduced MG30-based catalysts, and the images are displayed in Figure 8. Note that images for the Al_2O_3-based counterparts have been reported elsewhere, where large Pt particles of >100 nm size were observed already in the aged samples.[17] From Figure 8, the TEM images are fully consistent with the XRD results: (1) no Pt-containing crystals could be observed for the aged sample, suggesting Pt species that are highly dispersed, and (2) after reduction, Pt particles in the range of 5−10 nm are clearly evident. Consistent with the XRD and TEM results, NO oxidation results shown in Figure 7 also demonstrate that the NO oxidation activities for aged MG30-based samples fully recover after reduction.

From the XRD patterns displayed in Figure 6, the fresh and aged MG30-based samples appear to be rather similar, in which Pt is finely dispersed. However, these two catalysts have vastly different NO_x storage capacities. Unfortunately, conventional TEM is unable to image highly dispersed Pt species (see, for example, Figure 8a). In order to gain more information on their differences, HAADF-STEM with atomic resolution was employed to characterize the Pt species in fresh and aged Pt/K/MG30 (without a subsequent reduction treatment), and the results are shown in Figure 9. In these images, each white dot

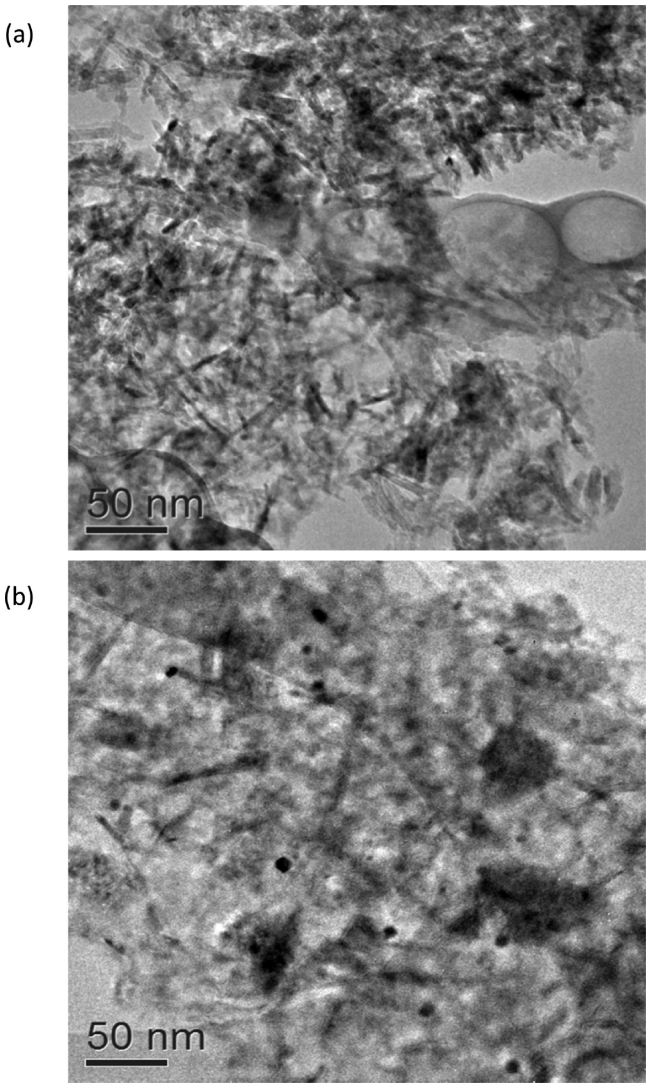

Figure 8. TEM images of the aged (a) and aged/reduced (b) 10K/Pt/MG30 samples.

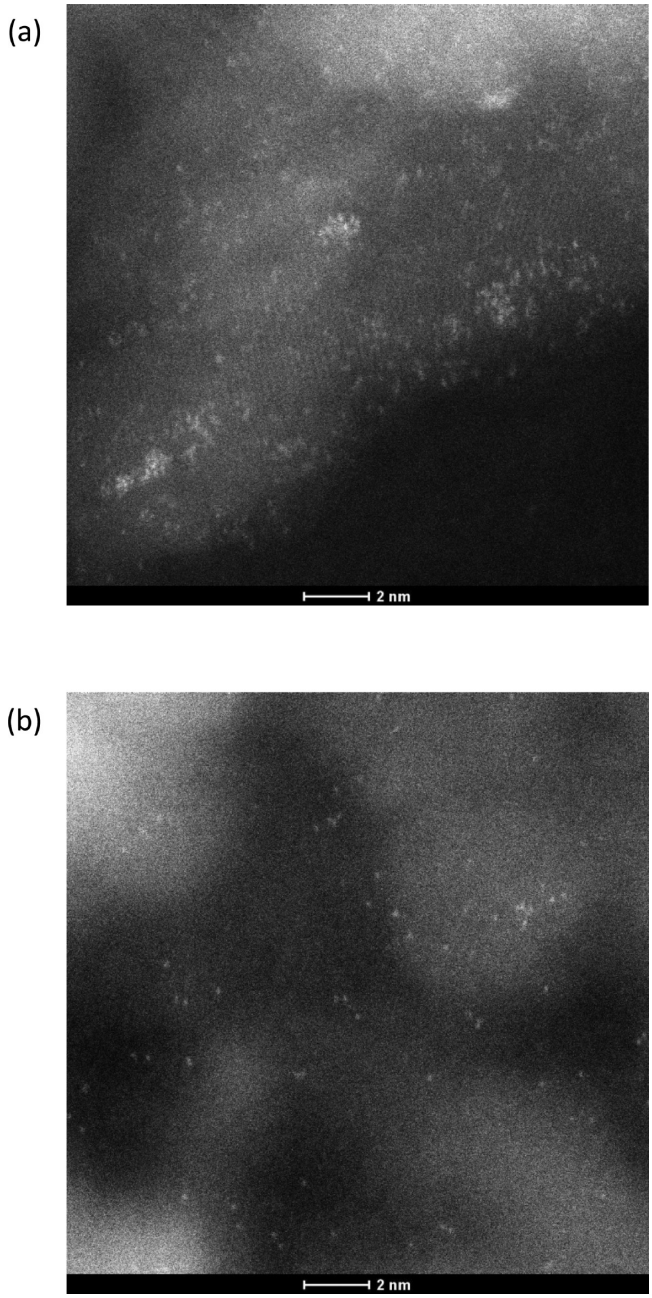

Figure 9. HAADF-STEM images of the fresh (a) and aged (b) 10K/Pt/MG30 samples.

DOI: 10.1021/acscatal.5b00542
ACS Catal. 2015, 5, 4680−4689

represents a Pt atom. In the fresh sample (Figure 9a), Pt is present in two forms: small clusters of ~1 nm and isolated atoms. In this case, since the support crystal plane is clearly visible, it can be deduced that a large portion of Pt appears to be dispersed on the surface of the support. However, for the aged sample, Pt could only be detected as single isolated atoms with much lower density (Figure 9b). These results perhaps suggest Pt diffusion into the support bulk during aging.

On the basis of the results shown above, it can be concluded that Pt oxidation is the major cause for degradation of the aged MG30-supported LNT catalyst. NO_x-TPD results, carried out after room-temperature NO_2 adsorption for the aged sample (data not presented here), show that most of the K (around 90%, relative to the fresh sample) is still accessible and can be utilized for NO_x storage. This demonstrates that changes in the K phase are not responsible for degradation during aging. Also, the aged-reduced MG30-based sample shows performance comparable to that of the fresh sample at high temperatures, further demonstrating that the potassium phase does not significantly degrade during aging. The aged-reduced MG30-based catalyst shows even better performance at temperatures below 450 °C, due to the fact that Pt is now fully reduced by the high-temperature treatment and regains NO oxidation capability, correspondingly promoting low-temperature NO_x trapping.

For the aged MG30-based sample, as already noted, a reduction treatment regenerates the NO_x storage capacity. It is worth mentioning that the reduction temperature must be sufficiently high. Notably, prior to each NO_x trapping measurement, all catalysts were first activated at 550 °C with multiple rich−lean cycling. This activation process appears to be sufficient for the fresh sample but is clearly insufficient for the aged samples, as evidenced by their poor performance. As such, the temperature-dependent Pt reduction was studied by in situ XAS, a powerful technique for monitoring the oxidation states of highly dispersed Pt.

XANES and EXAFS spectra for the fresh and aged MG30-supported samples, measured before and after reduction treatments, are shown in Figure 10. The high white line intensities for the fresh and aged catalysts are nearly identical and are indicative of oxidized Pt in a similar oxidation state. However, these spectra are quite different from that of a PtO_2 standard (data not shown). In particular, the XANES spectra for the fresh and aged catalysts are shifted to higher energy and show distinct oscillations after the while line, in contrast to that for PtO_2 suggesting that Pt is in a local environment different from that in PtO_2. Table 1 shows the EXAFS fitting results for the fresh and aged MG30-supported LNT catalysts on the basis of analyses of the spectra in the green and red curves of Figure 9b. The peak between 2.5 and 3.2 Å consists of contributions from Pt−Al (or Mg) and Pt−K scattering paths, and it was not possible to fit the spectra without both contributions. The results in Table 1 show that Pt is highly dispersed and is coordinated to the O and Al/Mg atoms from the support. Pt is also coordinated with K and, judging from the Pt−K bond disorder for the fresh catalyst, it appears that the structure consists of disordered Pt−K bonds or varying Pt−K bond lengths. The Pt−K coordination was more ordered after aging. The small increase in the Pt−Al/Mg coordination numbers suggests that aging resulted in more dispersed Pt and/or diffusion of Pt in the bulk of the $MgAl_2O_4$ spinel, although this is not conclusive due to the fairly large error bars for the Pt−Al/Mg coordination numbers.

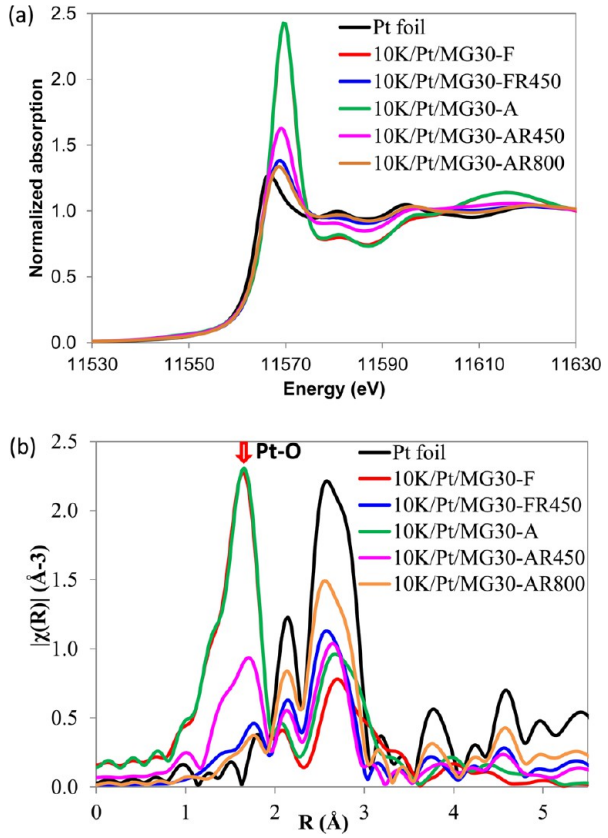

Figure 10. XANES (a) and EXAFS (b) spectra for fresh and aged 10K/Pt/MG30 after different treatments: fresh (F), fresh and reduced at 450 °C (FR-450), aged (A), aged and reduced at 450 °C (AR-450), and aged and reduced at 800 °C (AR-800).

The differences between the fresh and aged catalysts are pronounced after reduction, as is also illustrated in the Figure 9 XANES and EXAFS spectra. Notably, the white line intensity for the fresh catalyst (blue curve, Figure 9a) was much lower than that of the aged catalyst (pink curve) after a moderate (450 °C) temperature reduction treatment that is similar to conditions present during catalytic lean/rich cycling. This indicates that the catalyst aging increases the Pt dispersion and its interaction with the support, likely rendering it more difficult to reduce, a result also consistent with the catalytic activity data discussed above. The EXAFS fitting results in Table 1 provide more details on the catalysts after this 450 °C reduction. For example, the Pt−Pt coordination number for the fresh catalyst after 450 °C reduction is estimated to be 5.5, while it is only ~3.3 for the aged and mildly reduced sample. Additionally, it should be noted that, after reduction at 450 °C, the aged catalyst showed higher coordination with O and Al/Mg from the support in comparison with the fresh catalyst, which confirms that aging resulted in more dispersed Pt and/or diffusion of Pt in the bulk of the $MgAl_2O_4$ spinel.

Only after the aged Mg30-supported catalyst is reduced at high temperatures of 800 °C does the white line intensity decrease close to that of the fresh, reduced (at 450 °C) catalyst, indicating extensive Pt reduction. In fact, the EXAFS fitting results for the aged and high-temperature reduced catalyst show that Pt is essentially fully reduced after this 800 °C treatment; for example, no Pt coordination with O or Al from the support is evident. The Pt−Pt coordination number of 10.1 for this sample does indicate some sintering of Pt after the severe aging

DOI: 10.1021/acscatal.5b00542
ACS Catal. 2015, 5, 4680−4689

Table 1. EXAFS Fitting Results for Fresh and Aged Mg30-Supported LNT Catalysts

sample	pretreatment	absorber−backscatterer pair	CN	R (Å)	σ^2 (Å^2)	ΔE_0 (eV)	reduced χ^2
fresh	calcined at 600 °C	Pt−O	5.9(3)	2.006(4)	0.002(1)	9.8(7)	152
		Pt−Al/Mg	3.8(1.1)	2.96(2)	0.005(3)	9.8(7)	
		Pt−K	5.0(3.7)	3.22(4)	0.015(9)	9.8(7)	
fresh	reduced at 450 °C	Pt−O	1.0(2)	2.01(1)	0.003(2)	14.1(2.4)	29
		Pt−Pt	5.5(7)	2.755(3)	0.005(1)	8.5(1.5)	
		Pt−Al/Mg	1.6(7)	2.96(2)	0.006(6)	14.1(2.4)	
aged	calcined at 800 °C	Pt−O	5.8(3)	2.004(5)	0.002(1)	10.1(9)	229
		Pt−Al/Mg	4.7(1.2)	2.95(1)	0.004(2)	10.1(9)	
		Pt−K	2.0(6)	3.26(2)	0.004(4)	10.1(9)	
aged	reduced at 450 °C	Pt−O	2.9(3)	2.02(1)	0.004(1)	10.0(1.6)	110
		Pt−Pt	3.3(8)	2.749(9)	0.006(1)	4.1(2.3)	
		Pt−Al/Mg	3.2(4)	2.97(1)	0.003(3)	10.0(1.6)	
aged	reduced at 800 °C	Pt−Pt	10.1(8)	2.754(4)	0.006(1)	8.3(9)	54

and reduction treatments; however, as noted above, the extent of sintering was much lower than that of the Al_2O_3-supported sample.

In summary for this section, the XAS results confirm that Pt stays oxidized in both the fresh and the aged samples but that there exists a significant difference in terms of Pt reducibility. Because of the high dispersion and strong interactions between Pt and the support, a portion of Pt remains oxidized due to the coordination with O and Al/Mg from the support, even after a 450 °C reduction. Aging the catalyst results in increased Pt dispersion and possible diffusion into the bulk of the $MgAl_2O_4$ spinel. Consequently, the aged sample is even less reducible than the fresh catalyst at relatively low reduction temperatures. This leads to a loss of activity for NO oxidation and, correspondingly, a decrease in NO_x trapping performance. Instead, a much higher reduction temperature, notably 800 °C, is required to completely reduce Pt and regenerate the NO_x storage performance.

Overall, both Al_2O_3- and $MgAlO_x$-supported LNT catalysts degrade upon severe thermal aging, yet apparently via markedly different mechanisms. For Al_2O_3-based samples, relatively weak interactions between Pt and the support lead to severe Pt sintering during aging and irreversible deactivation of the catalyst. For MG30-based catalysts, on the other hand, strong interactions between Pt and the support cause Pt redispersion and even perhaps diffusion into the support bulk during oxidative aging, and a portion of this redispersed and/or bulk diffused Pt cannot be reduced during lean−rich cycling at 550 °C. This equally causes the Mg30-supported catalyst to lose NO oxidation activity and, correspondingly, NO_x storage performance. However, these aged catalysts can be regenerated via a high-temperature reduction treatment, while for Al_2O_3-based LNTs, Pt sintering during oxidative aging is essentially irreversible, and only very limited performance is restored by high-temperature reduction.

5. CONCLUSIONS

$MgAlO_x$ mixed oxides show at least two great advantages over conventional Al_2O_3 support materials for high-temperature LNT applications: (1) significantly improved NO_x trapping performance at high temperatures (at 450 °C and above), due to the enhanced stability of the stored nitrates and (2) minimized irreversible Pt sintering upon severe thermal aging treatments.

For fresh samples, results from Pt/K loading effects studies indicate that NO_x trapping is kinetically limited at low temperatures and thermodynamically limited at high temperatures. Therefore, the relative importance for Pt loading for NO_x storage decreases at elevated temperatures. Meanwhile, the best NO_x trapping performance is obtained at an optimized K loading, where a balance between the stability of nitrates and the extent of Pt exposure is maintained.

Thermal aging leads to decreased NO_x trapping performance for both Al_2O_3- and MG30-based catalysts, but this is due to apparently different mechanisms. For Al_2O_3-based catalysts, Pt sintering is the primary cause of degradation, while results presented here indicate that formation of highly dispersed oxidized Pt in MG30-based catalysts is responsible for decreased NO_x storage performance after aging. Such a difference is likely related to the varied extent of interactions between Pt and these two supports. Notably, for MG30-based catalysts, strong Pt−support interactions minimize the extent of Pt sintering. As such, a high-temperature reduction treatment recovers the NO_x storage performance of these MG30-supported LNTs.

AUTHOR INFORMATION

Corresponding Author

*E-mail for C.H.F.P.: Chuck.Peden@pnnl.gov.

Present Addresses

[†]Catalyst Technology & Integration, Cummins, Inc., 1900 McKinely Avenue, Columbus, Indiana 47201, United States.

[‡]Department of Chemical Engineering, Virginia Polytechnic Institute and State University, Blacksburg, Virginia 24061, United States.

Notes

The authors declare no competing financial interest.

ACKNOWLEDGMENTS

The authors gratefully acknowledge the US Department of Energy (DOE), Energy Efficiency and Renewable Energy, Vehicle Technologies Office, for primary support of this work. The electron microscopy measurements were also supported by the Chemical Imaging Initiative as part of the Laboratory Directed Research and Development (LDRD) Program at Pacific Northwest National Laboratory (PNNL). Most of the research described in this paper was performed in the Environmental Molecular Sciences Laboratory (EMSL), a national scientific user facility sponsored by the DOE's Office of Biological and Environmental Research and located at PNNL. PNNL is operated for the US DOE by Battelle. Use of the National Synchrotron Light Source, Brookhaven National

DOI: 10.1021/acscatal.5b00542
ACS Catal. 2015, 5, 4680−4689

Laboratory, for the XAS experiments was also supported by the US DOE, Office of Basic Energy Sciences (Grant No. DE-FG02-05ER15688). Beamline X-18A is supported, in part, by the Synchrotron Catalysis Consortium.

REFERENCES

(1) Epling, W. S.; Campbell, L. E.; Yezerets, A.; Currier, N. W.; Parks, J. E. *Catal. Rev.: Sci. Eng.* **2004**, *46*, 163−245.
(2) Choi, J. S.; Partridge, W. P.; Lance, M. J.; Walker, L. R.; Pihl, J. A.; Toops, T. J.; Finney, C. E. A.; Daw, C. S. *Catal. Today* **2010**, *151*, 354−361.
(3) Lietti, L.; Forzatti, P.; Nova, I.; Tronconi, E. *J. Catal.* **2001**, *204*, 175−191.
(4) Kim, D. H.; Mudiyanselage, K.; Szanyi, J.; Zhu, H.; Kwak, J. H.; Peden, C. H. F. *Catal. Today* **2012**, *184*, 2−7.
(5) Takeuchi, M.; Matsumoto, S. *Top. Catal.* **2004**, *28*, 151−156.
(6) Ogura, M.; Mozozumi, K.; Elangovan, S. P.; Tanada, H.; Ando, H.; Okubo, T. *Appl. Catal., B* **2008**, *77*, 294−299.
(7) Roy, S.; Vegten, N. van; Baiker, A. *J. Catal.* **2010**, *271*, 125−131.
(8) Wang, Q.; Chung, J. S. *Appl. Catal., A* **2009**, *358*, 59−64.
(9) Wang, Q.; Sohn, J. H.; Chung, J. S. *Appl. Catal., B* **2009**, *89*, 97−103.
(10) Shen, W.; Nitta, A.; Chen, Z.; Eda, T.; Yoshida, A.; Naito, S. *J. Catal.* **2011**, *280*, 161−167.
(11) Takahashi, N.; Matsunaga, S.; Tanaka, T.; Sobukawa, H.; Shinjoh, H. *Appl. Catal., B* **2007**, *77*, 73−78.
(12) Kwak, J. H.; Kim, D. H.; Szanyi, J.; Cho, S. J.; Peden, C. H. F. *Top. Catal.* **2012**, *55*, 70−77.
(13) Tanaka, H.; Taniguchi, M.; Uenishi, M.; Kajita, N.; Tan, I.; Nishihata, Y.; Mizuki, J.; Narita, K.; Kimura, M.; Kaneko, K. *Angew. Chem., Int. Ed.* **2006**, *45*, 5998−6002.
(14) Hatanaka, M.; Takahashi, N.; Takahashi, N.; Tanabe, T.; Nagai, Y.; Suda, A.; Shinjoh, H. *J. Catal.* **2009**, *266*, 182−190.
(15) Tanabe, T.; Nagai, Y.; Dohmae, K.; Sobukawa, H.; Shinjoh, H. *J. Catal.* **2008**, *257*, 117−124.
(16) Li, W. Z.; Kovarik, L.; Mei, D.; Liu, J.; Wang, Y.; Peden, C. H. F. *Nat. Commun.* **2013**, *4*, 2481.
(17) Luo, J.; Gao, F.; Kim, D. H.; Peden, C. H. F. *Catal. Today* **2014**, *231*, 164−172.
(18) Karim, A. M.; Howard, C.; Roberts, B.; Kovarik, L.; Zhang, L.; King, D. L.; Wang, Y. *ACS Catal.* **2012**, *2*, 2387−2394.
(19) Ravel, B.; Newville, M. *J. Synchrotron Radiat.* **2005**, *12*, 537−541.
(20) Newville, M. *J. Synchrotron Radiat.* **2001**, *8*, 96−100.
(21) Zabinsky, S. I.; Rehr, J. J.; Ankudinov, A.; Albers, R. C.; Eller, M. J. *Phys. Rev. B: Condens. Matter Mater. Phys.* **1995**, *52*, 2995−3009.
(22) Zhai, Y. P.; Pierre, D.; Si, R.; Deng, W. L.; Ferrin, P.; Nilekar, A. U.; Peng, G. W.; Herron, J. A.; Bell, D. C.; Saltsburg, H.; Mavrikakis, M.; Flytzani-Stephanopoulos, M. *Science* **2010**, *329*, 1633−1636.
(23) Liu, Y.; Meng, M.; Zou, Z.; Li, X.; Zha, Y. *Catal. Commun.* **2008**, *10*, 173−177.
(24) Kim, D. H.; Mudiyanselage, K.; Szanyi, J.; Kwak, J. H.; Zhu, H.; Peden, C. H. F. *Appl. Catal., B* **2013**, *142−143*, 472−478.
(25) Yuvaraj, S.; Lin, F. Y.; Chang, T. H.; Yeh, C. T. *J. Phys. Chem. B* **2003**, *107*, 1044−1047.
(26) Kwak, J. H.; Mei, D.; Yi, C. W.; Kim, D. H.; Peden, C. H. F.; Allard, L. F.; Szanyi, J. *J. Catal.* **2009**, *261*, 17−22.
(27) Minemura, Y.; Ito, S.; Miyao, T.; Naito, S.; Tomishige, K.; Kunimori, K. *Chem. Commun.* **2005**, *11*, 1429−1431.
(28) Xu, J.; Harold, M. P.; Balakotaiah, V. *Appl. Catal., B* **2011**, *104*, 305−315.
(29) Kabin, K. S.; Muncrief, R. L.; Harold, M. P.; Li, Y. *Chem. Eng. Sci.* **2004**, *59*, 5319−5327.
(30) Kabin, K. S.; Khanna, P.; Muncrief, R. L.; Medhekar, V.; Harold, M. P. *Catal. Today* **2006**, *114*, 72−85.
(31) Kumar, A.; Harold, M. P.; Balakotaiah, V. *J. Catal.* **2010**, *270*, 214−223.
(32) Bhatia, D.; McCabe, R. W.; Harold, M. P.; Balakotaiah, V. *J. Catal.* **2009**, *266*, 106−119.
(33) Olsson, L.; Fridell, E. *J. Catal.* **2002**, *210*, 340−353.

DOI: 10.1021/acscatal.5b00542
ACS Catal. 2015, 5, 4680−4689